

# Zero Sound Attenuation near the Quantum Limit in Normal Liquid $^3\text{He}$ close to the Superfluid Transition

Brian C. Watson,\* Naoto Masuhara, and Mark W. Meisel

*Department of Physics and the Center for Condensed Matter Sciences,  
Microkelvin Research Laboratory, University of Florida, Gainesville, FL 32611-8440, USA*

(Dated: October 29, 2018)

## Abstract

The zero sound attenuation of normal liquid  $^3\text{He}$  has been studied over a range of temperatures from slightly above the superfluid transition temperature,  $T_c$ , to approximately 10 mK at the constant pressures of 1 bar and 5 bar. Using longitudinal  $\text{LiNbO}_3$  transducers, operating both on and off resonance, the experiment was performed at 15 discrete frequencies located in several broadband frequency windows, including 16 – 25 MHz, 60 – 70 MHz, and 105 – 111 MHz. The results are compared to Landau's prediction for the attenuation of zero sound in the quantum limit, ( $k_B T \ll \hbar\omega \ll k_B T_F$ ), where  $\alpha_0(P, T, \omega) = \alpha'(P) T^2 \{1 + (\hbar\omega/2\pi k_B T)^2\}$ . Calibration of the received zero sound signals was performed by measuring the temperature dependence of the first sound attenuation from 30 mK to 800 mK at those same frequencies and pressures. The data are compared to previous results.

PACS numbers: 67.50.Dg

## I. INTRODUCTION

In 1957, Landau established the foundations of a phenomenological theory used to describe strongly interacting Fermi systems.<sup>1,2</sup> Commonly referred to as Landau Fermi Liquid Theory, this theory has provided an extremely successful description of normal liquid  $^3\text{He}$  and some properties of superfluid  $^3\text{He}$ , and it has also been extended to electron systems in some metals.<sup>3,4,5,6,7,8,9</sup> Within the framework of this theory, quantum kinetic equations for Fermi liquids often reduce to classical kinetic equations, and the subtle differences between these two limits is not easily detected experimentally. However, a significant difference is expected to appear in the attenuation of zero sound in normal liquid  $^3\text{He}$  when  $2\pi k_B T \simeq \hbar\omega$ , where  $\omega = 2\pi f$  is the angular frequency of the sound excitation.

In this paper, we provide a detailed description of our attempt to study the quantum limit of zero sound attenuation. The next section reviews the nature of zero sound and the previous attempts to measure the attenuation in the quantum limit. This introductory material is followed by an overview of our general approach to the experiment and the analysis of the results, especially the calibration necessary to obtain the absolute attenuation of the liquid. The presentation continues with a description of our experimental cell and acoustic techniques. Next, our data in the zero sound and first sound regimes will be presented, and then our analysis of data will be provided. Finally, we will conclude with a discussion of the present state of our results.

## II. REVIEW OF ZERO SOUND AND ATTENUATION STUDIES

In his pioneering work, Landau also identified a new type of sound mode which is known as zero sound. Distinct from ordinary hydrodynamic or first sound, zero sound occurs when the standard quasiparticle collisions can no longer provide the necessary restoring force to the system. However, even in this “collisionless” regime, the quasiparticles experience restoring forces which attempt to return the system to equilibrium. These forces arise from the interactions of the quasiparticles and enable the propagation of zero sound. More specifically, the first sound regime exists when  $\omega\tau \ll 1$  while zero sound propagates when  $\omega\tau \gg 1$ , where  $\tau$  is the quasiparticle collision time which is theoretically predicted to be proportional to  $T^{-2}$ . Consequently, by fixing the frequency of the probing sound wave and

sweeping the temperature under the appropriate conditions, the theory predicts a crossover from zero sound to first sound when  $\omega\tau = 1$ . The theoretical predictions for the attenuation of zero and first sound may be written, respectively, as

$$\alpha_0(P, T) = \alpha'(P) T^2 \quad \text{for} \quad \frac{1}{\tau} \ll \omega \quad , \quad (1)$$

and

$$\alpha_1(P, T, \omega) = \alpha''(P) \left( \frac{\omega^2}{T^2} \right) \quad \text{for} \quad \omega \ll \frac{1}{\tau} \quad , \quad (2)$$

where  $\alpha'$  and  $\alpha''$  are appropriate pressure-dependent parameters.<sup>6</sup> In 1963, through the use of acoustic impedance techniques, Keen, Matthew, and Wilks experimentally verified the existence of a crossover from first to zero sound.<sup>15</sup> The first direct observation of the first to zero sound regimes and the predicted behavior for the attenuation was reported in 1966 by Abel, Anderson, and Wheatley.<sup>16</sup> Since this early work, numerous workers have measured  $\alpha'$ , which is strongly pressure dependent. The experiments reported herein have allowed us to determine  $\alpha'(P)$  at 1 bar and 5 bar. In Appendix A, our values are combined with the results of other groups,<sup>17,18,19,20,21</sup> and interpolation formula are presented for  $\alpha'$  as a function of pressure and molar volume ranging from saturated melting pressure to the melting curve.

An additional important prediction of Landau Fermi Liquid Theory is the behavior of the zero sound attenuation in the limit  $\hbar/\tau \ll k_B T \ll \hbar\omega \ll k_B T_F$ . When  $\hbar/\tau \ll \hbar\omega \ll k_B T$ , the scattered quasiparticles remain within the thermally broadened Fermi surface. Due to the successive thermal collisions, the quantum mechanical features of the individual processes are smeared out. In this case which Landau referred to as the ‘‘classical’’ limit,<sup>2</sup> the thermal collision rate simply determines the absorption of the ultrasound as expressed in Eq. (1), and the sound attenuation vanishes if this condition is extrapolated to the zero temperature limit. On the other hand when  $\hbar\tau \ll k_B T \ll \hbar\omega \ll k_B T_F$ , the quasiparticles are scattered away from the Fermi surface and remain in non-equilibrium states for a longer time due to the scarce collision probability. In this case which Landau referred to as the ‘‘quantum’’ regime,<sup>2</sup> the quantum mechanical features of each process are non-negligible, and the sound attenuation is dependent on phonon energy or frequency, but not the temperature. Landau derived a result which covers both limits continuously,<sup>2</sup> namely

$$\alpha_0(P, T, \omega) = \alpha'(P) T^2 \left\{ 1 + \left( \frac{\hbar\omega}{2\pi k_B T} \right)^2 \right\} \quad \text{for} \quad k_B T \ll \hbar\omega \ll k_B T_F \quad . \quad (3)$$

Thus, the transition from the classical to the quantum regimes is expected to occur when  $\hbar\omega \approx 2\pi k_B T$ . This result has been discussed often in the literature;<sup>6,8,22,23,24</sup> however, in spite of efforts by (probably) every experimental group that ever propagated ultrasound in normal liquid  $^3\text{He}$  below 10 mK, this prediction remains experimentally unverified, although some preliminary evidence for the “quantum” limit has been reported.<sup>25,26,27,28</sup> These preliminary reports are summarized in Table I, where the theoretically predicted quantum term is calculated for comparisons of its size to unity, Eq. (3).

The reasons for the null or quantitatively uncertain experimental results are easy to understand. Ideally speaking, the highest frequencies ( $\gg 1$  GHz) and the lowest temperatures ( $\ll 1$  mK) are required to conclusively confirm the quantum limit. Unfortunately, the highest frequency measurements are limited by experimental constraints and the lowest temperatures are bounded by the superfluid transition. Consequently, measurements have been restricted to the “*transition region*”, *i.e.* between the classical and quantum limits, where the absolute values of attenuation are necessary for quantitative arguments (see Table I). Within the “*transition region*”, Eq. (3) is considered to be valid, but a detailed study has not yet been made. One way to think of the experiment is in the form of the measured attenuation,  $\alpha_m$ , plotted as a function of  $T^2$ . In other words, rewriting Eq. (3) gives

$$\alpha_m(P, T, \omega) = \alpha'(P) T^2 + \alpha'(P) \left( \frac{\hbar \omega}{2\pi k_B} \right)^2 + \alpha_{bk}(\omega) \quad , \quad (4)$$

where  $\alpha_{bk}$  is the parasitic background attenuation and all the temperature, pressure, and frequency dependences have been shown explicitly. For a positive result, the experiments must unambiguously identify a non-zero y-intercept, on an  $\alpha_m$  *vs.*  $T^2$  plot, that is larger than the background contribution. The major obstacle in all of the experiments (Table I) is to reliably determine the background attenuation, and undoubtedly more effort is required to overcome the difficulties in determining the absolute values of the attenuation. Any possible pressure dependence of  $\alpha_{bk}$  will be discussed when appropriate.

### III. OVERVIEW OF GENERAL APPROACH

The general strategy for measuring the quantum term in zero sound uses the temperature dependence of first sound to calibrate the signal levels and involves several steps. Essentially, we must fit the temperature dependence of the first sound amplitude to a known expression

to determine the absolute attenuation in both the first and zero sound regimes. The process of converting the raw zero sound data into absolute attenuation is summarized in the flow chart shown in Fig. 1. Here, we sketch the general plan, and the details for will be given in the following sections.

Naturally, the first steps involve the acquisition of the experimental signals, and standard procedures are used to subtract crosstalk and to integrate the received pulses. Further analysis requires values for the longitudinal viscosity at 1 bar and 5 bar, and we have used the data reported by Bertinat *et al.*<sup>29</sup> and Nakagawa *et al.*<sup>30</sup> Using this viscosity, we subtract a correction due to the walls of the cylindrical sample cell from the first sound raw data. Applying the wall correction at this stage of the analysis decreases the number of independent variables and improves the quality of the subsequent fits. Next, the temperature dependence of the first sound data must be fit to obtain the frequency dependent factor,  $F(\omega)$ . The fits were performed on the natural logarithm of the amplitude as a function of temperature so that the factor,  $F(\omega)$ , represents a constant vertical shift. Several additional properties of the liquid are required to calculate the first sound attenuation, including density,  $\rho$ , thermal conductivity,  $\kappa(T)$ , isothermal and isobaric specific heats,  $c_v(T)$  and  $c_p(T)$ , first sound velocity,  $C_1$ , and second viscosity  $\eta(T)$ . The first sound velocity,  $C_1$ , is determined directly from the data by measuring time-of-flight of first sound pulses. The second viscosity is generally assumed to be small and negligible relative to the other contributions.<sup>6,32</sup> The remaining properties have been calculated by Kollar and Vollhardt<sup>31</sup> using a consistent set of thermodynamic quantities. The pressure dependent factor  $\alpha'(P)$  is determined by a linear fit to the natural logarithm of the zero sound data plotted as a function of the square of temperature. Once this value and the frequency dependent factor  $F(\omega)$  are known, the zero sound data can be dissected for evidence of additional attenuation that may be due to the quantum limit.

#### IV. EXPERIMENTAL DETAILS

The experiment was performed using the same cylindrical sample cell employed in the previous experiment;<sup>28</sup> however, the transducers and Macor spacer are different. Details of the acoustic technique, including the transducers, spectrometer, cell dimensions, and thermometry have been reported elsewhere,<sup>33,34</sup> so only the salient aspects will be given here.

## A. Sample Cell and Thermometry

The experimental activity was divided into two separate stages with the sample cell pressure fixed at either 1 bar or 5 bar. The cell pressure was changed using a standard zeolite absorption dipstick and was monitored by a Digiquartz transducer. After the desired pressure was set, a room temperature valve was closed at the top of the cryostat. For this experiment, the pressure was not measured *in situ*, but a low temperature pressure gauge was added and used in subsequent work. The volume of the capillary line between the top of the cryostat and the  $^3\text{He}$  cell will produce a small change in the cell pressure which will be considered in our analysis.

The sample cell was placed in a silver tower mounted on a copper plate attached to the top of the copper demagnetization stage. Further details of this cryostat design are described elsewhere.<sup>35</sup> A silver powder heat exchanger in the silver tower provides thermal contact for cooling the liquid sample. Miniature coaxial cables with a superconducting core and a CuNi braid were used between the tower and the 1 K pot. Stainless steel semi-rigid coaxial cables were used from the 1 K pot to the room temperature connectors. Above 40 mK, the temperature was measured using a calibrated ruthenium oxide ( $\text{RuO}_2$ , Dale RC-550) resistor which has a resistance of  $\approx 500 \Omega$  at ambient temperature.<sup>36</sup> The value of this  $\text{RuO}_2$  thermometer was measured using an AC resistance bridge (Linear Research). A heater mounted on the nuclear stage supplied up to  $1 \mu\text{W}$  of thermal power. From 40 mK to 1 mK, the temperature was measured using a  $^3\text{He}$  melting curve thermometer. This experiment used the  $^3\text{He}$  melting curve described by Ni *et al.*,<sup>37</sup> which is consistent with the Greywall scale.<sup>11</sup> Since the melting curve determined by Ni and co-workers did not extend much above the minimum in the melting curve, the scale given by Grilly<sup>38</sup> was used above 325 mK. The resultant temperature calibration from the Grilly scale was adjusted by a constant to match the value of the minimum of melting curve as given by Ni *et al.* Below nominally 3 mK, a Pt wire NMR thermometer (PLM-3, Instruments of Technology, Finland) was used and calibrated against the  $^3\text{He}$  melting curve thermometer.

## B. Acoustic Techniques, Path Length, and Dynamic Range

A commercial Tekmag NMR spectrometer was used for the present work, and this arrangement allowed for phase sensitive detection.<sup>34</sup> Our configuration contrasts with the experiments conducted by Granroth *et al.*,<sup>28</sup> who employed Matec electronics (Models 310 and 625) for amplitude detection. For our study, a typical pulse sequence consisted of 64 pulses with 4 s delay between each pulse. A phase cycling procedure was used for averaging over multiples of four pulses and a relatively long 4  $\mu$ s pulse was used to limit the frequency bandwidth of the transmitted pulses. The in-phase and quadrature components were separately digitized at 10 Msamples/s and 2048 samples were recorded for each pulse. Between each pulse sequence, there was at least 8 minutes delay to avoid heating the liquid. Before and after the acquisition of each data set, the temperature value was recorded and averaged to account for any temperature drift. The output level of the spectrometer was fixed at approximately 13 dBm (maximum) during the experiment so that comparisons between received signal levels could be performed. To avoid heating the liquid, a variable inline attenuator (set at  $-20$  dB) was used on the transmitter side so that the cumulative attenuation from the cables provided a pulse input power of approximately 1 nJ. To test for linearity, signals were averaged at fixed frequency and temperature using different attenuator values.<sup>34</sup>

The received amplitude of a 16 MHz pulse as a function of time at a pressure of 1 bar and a temperature of 1.11 mK is shown in Fig. 2(A). The coherent noise due to electrical feedthrough is evident in the first 10  $\mu$ s of data. To improve the signal to noise ratio, a reference signal was taken at 3.52 mK (Fig. 2(B)), where the received pulse amplitude cannot be differentiated from the noise, and was subsequently subtracted from all of the zero sound data at 1 bar. The real and imaginary portions of the signal were subtracted separately before calculating the magnitude. The result after subtraction is shown in Fig. 2(C), where the crosstalk feature at approximately 7  $\mu$ s has clearly been removed. Prior to any further analysis, a similar procedure was performed for the zero sound data at 5 bar and the first sound data at both pressures. The integration of the received pulses was performed over only a 4  $\mu$ s area. Furthermore, the uncertainty for each integration was determined by integrating a 4  $\mu$ s area located near 200  $\mu$ s, *i.e.* near the end of the data acquisition.

The absolute attenuation is linearly dependent on the path length, and therefore an *in situ*

measurement of this length is desirable. The response observed from a 22 MHz pulse at 5 bar and 1.55 mK is shown in Fig. 3. The time length between successive echoes, combined with the tabulated velocity of zero sound,<sup>12</sup> allow us to calculate a path length,  $\ell$ , of

$$\ell = 0.327 \pm 0.002 \text{ cm} . \quad (5)$$

The uncertainty in this measurement is primarily determined by the 100 ns time resolution of the spectrometer. This determination of  $\ell$  was then combined with the data in the first sound regime to obtain values for  $C_1(P, T)$ . These values are in agreement with published values, within the uncertainty. The temperature and pressure dependences of  $C_1$  are required for the calibration of the absolute attenuation, and additional details are given in Appendix B.

The dynamic range of our attenuation measurement is restricted by our input power and cell size. Figure 4 shows the attenuation as a function of the logarithm of temperature at a pressure of 1 bar and a frequency of 16 and 64 MHz. The attenuation on the left and right side of Fig. 4 is due to zero sound and first sound, respectively. The absolute attenuation (y-axis) has been determined by fitting the temperature dependences of the zero sound and first sound data to known expressions. If the attenuation is smaller than approximately  $0.4 \text{ cm}^{-1}$ , then changes in the attenuation will be smaller than the scatter due to the noise (lower horizontal line). If the attenuation is larger than  $16.2 \text{ cm}^{-1}$  then the signal will not be detected (upper horizontal line).

## V. ZERO SOUND

Typical received amplitudes as a function of time and temperature for zero sound at 10 MHz and 1 bar are shown in Fig. 5. The crosstalk has been subtracted using the method discussed in the previous section. The decrease in amplitude is due to the  $T^2$  dependence of attenuation on temperature. At low frequency, 8, 10, and 16 MHz, the transducer response is broader and hence the received pulses resemble the square transmitted pulse. Higher frequency received pulses,  $f > 19$  MHz, contain sharp peaks related to the transducer responses at that frequency.<sup>33</sup>

In order to accurately measure the absolute attenuation of zero sound, we must determine the large frequency dependence due to the transducer response. Consequently, it is necessary to compare the zero sound signal levels with the high temperature, low attenuation limit of



first sound.

## VI. FIRST SOUND

In order to accurately determine the zero sound attenuation, we must calibrate the large frequency dependence of the transducer response by studying the attenuation of first sound. Herein lies the greatest uncertainty or propagation of systematic errors.

The first sound attenuation was measured at fixed temperatures in the range from approximately 30 mK to 800 mK at two different pressures. For these measurements, 21 and 27 discrete temperatures were used at 1 bar and 5 bar, respectively. As in the previous section, low temperature ( $T \approx 30$  mK), high attenuation data were subtracted from all other data to eliminate the contribution from electrical crosstalk. The integration of the received signals was performed over a 4  $\mu$ s window which was adjusted to compensate for the pressure being studied since the speed of sound changed. The noise level for each integration was produced by a further integration over a 4  $\mu$ s region at  $t = 200$   $\mu$ s.

The attenuation of first (hydrodynamic) sound can be written as

$$\alpha_1(P, T, \omega) = \frac{\omega^2}{2\rho C_1^3} \left[ \left( \frac{4}{3}\eta + \zeta \right) + \kappa \left( \frac{1}{c_v} - \frac{1}{c_p} \right) \right] \approx \frac{2\omega^2\eta}{3\rho C_1^3} \propto \frac{\omega^2}{T^2} \quad , \quad (6)$$

where  $\eta$  and  $\zeta$  are the first (longitudinal) viscosity and second (bulk) viscosity,  $\kappa$  is the thermal conductivity,  $\rho$  is the density,  $C_1$  is the sound velocity, and  $c_v$  and  $c_p$  are the specific heats at constant volume and pressure.<sup>39</sup> As mentioned previously, the first sound velocity,  $C_1$ , is determined using the time delay between the arrival of the received pulse and the length of the cell. The thermal conductivity,  $\kappa$ , and the specific heat at constant volume,  $c_v$ , have been measured by Greywall.<sup>11,40</sup> Using the measurements of Greywall, Kollar and Vollhardt<sup>31</sup> have calculated the density,  $\rho$ , and specific heat at constant pressure,  $c_p$ , using a consistent set of thermodynamic quantities. The contribution to the attenuation from the thermal conductivity is expected to be significant as it has a linear dependence on temperature and a quadratic dependence on frequency. Therefore, a term corresponding to the thermal conductivity must be included when fitting the temperature dependence of first sound attenuation to a known expression.

An additional attenuation correction, which accounts for scattering of the quasiparticles

on the walls of the cylindrical cell,<sup>39,41</sup> can be written as

$$\alpha_{wall} = \frac{\omega}{2RC_1} \left[ \frac{2\eta}{\rho\omega} \right]^{1/2}, \quad (7)$$

where  $R$  is the radius of the cell. For a frequency of 10 MHz and a temperature of 800 mK, the attenuation due to the wall scattering is 14% of the hydrodynamic attenuation. To improve fitting accuracy, for all of the data presented, the wall attenuation was subtracted from the data before fitting to the attenuation in Eq. (6). By combining Eq. (6) with an additional frequency dependent factor, we can write the amplitude of first sound,  $\mathcal{A}_1$ , (recalling that the crosstalk and wall attenuation corrections have already been made) as

$$\mathcal{A}_1 = F(\omega) \exp \left\{ -\frac{\omega^2 \ell}{2\rho C_1^3} \left[ \left( \frac{4}{3}\eta + \zeta \right) + \kappa \left( \frac{1}{c_v} - \frac{1}{c_p} \right) \right] \right\}, \quad (8)$$

where  $F(\omega)$  is the frequency dependence of the transducer and the related electronics. The factor  $F(\omega)$  is the only unknown quantity in Eq. (8) and hence is uniquely determined by fitting Eq. (8) to the data. It is important to note that the terms inside the exponential in Eq. (8) decrease as the temperature is increased but they do not become arbitrarily small. In other words,  $F(\omega)$  cannot be determined by simply taking the  $T \rightarrow 0$  limit. Finally, once  $F(\omega)$  is determined from Eq. (8), the amplitude of zero sound can be written as

$$\mathcal{A}_0 = F(\omega) \exp \left\{ -\alpha'(P) T^2 \ell \left[ 1 + \left( \frac{\hbar\omega}{2\pi k_B T} \right)^2 \right] \right\}. \quad (9)$$

The longitudinal viscosity,  $\eta$ , has been measured by several research groups<sup>29,30,42,43</sup> over various temperature ranges and pressures. At temperatures above 100 mK, experimental data<sup>29,42</sup> indicate that  $\eta$  deviates from pure  $1/T^2$  behavior, and the temperature dependence of  $\eta$  has the form

$$\eta(P) = \frac{\Gamma_1(P)}{T^2} + \frac{\Gamma_2(P)}{T^n}, \quad (10)$$

where  $\Gamma_1$ ,  $\Gamma_2$ , and  $n$  are constants. We are unable to determine the second constant,  $\Gamma_2$ , directly from our data, and both previous measurements<sup>29,42</sup> of this term have been performed only at saturated vapor pressure. Consequently, some assumptions and an interpolation of the reported viscosity values are required.

For our analysis, the first constant,  $\Gamma_1(P)$ , was taken from the results of Nakagawa *et al.*<sup>30</sup> who worked over a wide range of pressures. The second constant,  $\Gamma_2$ , was obtained from the value reported by from Bertinat *et al.*,<sup>29</sup> after it was multiplied by the same factor necessary

to make their  $\Gamma_1$  term equal to the  $\Gamma_1$  term reported by Nakagawa *et al.* at either 1 bar or 5 bar. This correction was necessary since Bertinat *et al.* only worked at saturated vapor pressure. With this approach, we are assuming that the pressure dependences of  $\Gamma_1$  and  $\Gamma_2$  are identical and that the temperature dependence of the second term,  $1/(T^{0.42})$ , is independent of pressure. With this interpolation procedure, the final result for the viscosity expressed in poise (P) is

$$\eta(P = 1 \text{ bar}) = \frac{1.99}{T^2} + \frac{4.44 \times 10^{-4}}{T^{0.42}} \quad (11)$$

at 1 bar and

$$\eta(P = 5 \text{ bar}) = \frac{1.62}{T^2} + \frac{3.62 \times 10^{-4}}{T^{0.42}} \quad (12)$$

at 5 bar, where  $T$  has units of mK. We have more confidence in the value of  $\Gamma_2$  at 1 bar than at 5 bar because the pressure is closer to saturated vapor pressure.

An expression for the second or bulk viscosity,  $\zeta$ , has been derived by Sykes and Brooker<sup>32</sup> in terms of a collision integral; however in their analysis, no attempt was made to evaluate the expression numerically. Although it has generally been assumed that the second viscosity has a  $\zeta \sim T^0$  dependence, they predict that the second viscosity has a  $\zeta \sim T^2$  dependence. It should be noted that their calculation relies on the assumption that  $^3\text{He}$  is well described by Fermi liquid theory which is not necessarily valid above the temperature of approximately 150 mK ( $T \approx T_F/10$ ). In addition, the magnitude of the second viscosity at temperatures below 1 K is expected to be negligible,<sup>23</sup> so we have not included it in our analysis.

To summarize, it is noteworthy that Eqs. (11) and (12) are self-consistent with our measurements of the attenuation of first sound.<sup>34</sup> This point is illustrated in Fig. 6, where the first sound data are well described by Eq. (8) when using the viscosity given by Eq. (11). Alternatively, if the values for the viscosity are interpolated from the data reported by Bertinat *et al.*<sup>29</sup> and Carless *et al.*,<sup>43</sup> as was done by Granroth and co-workers,<sup>28</sup> the present data are not well fit, Fig. 6. The present work represents an improvement over the results reported by Granroth *et al.* since the number of temperatures investigated was increased by approximately 3 and the uncertainty limits were reduced by a factor of about 2.

## VII. ADDITIONAL UNCERTAINTIES AND ANALYSIS

To this point, our analysis have not addressed three important sources of uncertainty, namely the nonparallelism of the transducers, the measurement and stability of the pressure, and the variation of the acoustic impedance.

The nonparallelism of the transducers will add an additional frequency dependent factor,  $N(\omega)$ , to the zero and first sound amplitudes, so the received amplitude is related to the transmitted amplitude as<sup>44,45</sup>

$$\mathcal{A}_{rec} = \mathcal{A}_{trans} N(\omega) e^{-\alpha \ell} . \quad (13)$$

The factor  $N(\omega)$  is expressed in terms of a Bessel function

$$N(\omega) = 2 \frac{J_1 \left[ (2m - 1) \frac{\omega}{c} R \Theta \right]}{(2m - 1) \frac{\omega}{c} R \Theta} , \quad (14)$$

where  $\Theta$  is the angular error and  $m$  is the received pulse number. In a previous experiment,<sup>28</sup> the nonparallelism was determined by filling the cell with  $^4\text{He}$  and measuring the attenuation of closely spaced frequencies from 8 to 64 MHz. However, for the present experiment, the transducer properties could not accommodate a continuous sweep of the frequency. Therefore the uncertainty due to nonparallelism must be estimated. Fortunately, the uncertainty due to nonparallelism will occur in both the zero and first sound regimes, and the effect will partially cancel. Nevertheless, the sound velocity change between zero and first sound will cause the zeros in the Bessel function to appear at slightly different frequencies. A relatively small increase in the nonparallelism will result in a large increase in the uncertainty at high frequencies. In addition, at specific frequencies that correspond to a zero in the Bessel function, the uncertainty will increase dramatically. The uncertainty at 5 bar is less than the uncertainty at 1 bar because there is less difference between the first sound and zero sound velocities at that pressure. In the previous experiment by Granroth *et al.*,<sup>28</sup> the value of  $\Theta$  was measured as  $(4.1 \pm 0.1) \times 10^{-4}$  radians, which is consistent with uncertainties due to machining. For the present experiment, the nonparallelism is assumed to be the same as the previous measurement by Granroth *et al.* and the corresponding uncertainty is estimated as  $\pm 20\%$  of the final result at 1 bar and  $\pm 10\%$  at 5 bar. These percentage values appear to be large only because the quantum term in zero sound attenuation is exceedingly small.

There are two sources of uncertainties that are related to pressure changes in the cell. First, there are pressure changes due to variations in temperature. Second, there are pressure

changes due to the cyclical change (period of 3 days) of the  $^4\text{He}$  level in the dewar. The pressure change produced by a variation in temperature was measured in a subsequent experiment using a strain gauge attached to the  $^3\text{He}$  cell. It is difficult to calculate the effect of the pressure change on the transducer properties. However, we can estimate the uncertainty in the amplitude due to the temperature variation as approximately  $\pm 4\%$  in the first sound regime. In comparison, the pressure change due to the  $^4\text{He}$  level in the dewar is significantly less, with the error of approximately  $\pm 1\%$  of the first sound amplitude.

There is an additional correction due to a change in the acoustic impedance of liquid  $^3\text{He}$ . The amount of energy that is transmitted into the  $^3\text{He}$  cell is a function of the impedance of the transducers and the  $^3\text{He}$  liquid. The real component of the impedance of a hydrodynamic fluid can be written as

$$\text{Re}[Z] = \rho(T, P) C(T, P) \quad , \quad (15)$$

where  $\rho(T, P)$  is the density of the liquid and  $C(T, P)$  is the sound velocity. Between zero sound and first sound, there is a significant increase in the sound velocity and a subtle change in  $\rho$  combining to cause an increase in acoustic impedance. Independent of frequency, the overall signal amplitude will decrease in the first sound regime. Accordingly, a constant adjustment must be applied to the first sound data to force a zero intercept in a linear fit of the data in Figs. 7 and 8. The constant adjustment is  $0.466 \text{ cm}^{-1}$  and  $0.537 \text{ cm}^{-1}$  for the 1 bar and 5 bar data, respectively. The ratio between these two values ( $0.537/0.436$ ) = 1.15 is roughly equal to the ratio between the calculated values of  $[\rho C(5 \text{ bar})]/[\rho C(1 \text{ bar})]$  = 1.38.

## VIII. FINAL RESULTS AND DISCUSSION

After all the analysis, the received zero sound signals yield a corrected attenuation,  $\alpha_{\text{cor}}$ , which should represent the absolute attenuation of the liquid. From Eq. (3), the final results may be plotted in the form  $[\alpha_{\text{cor}}/\alpha' T^2] T^2 - 1$  vs.  $(\omega/2\pi)^2$ , as shown in Fig. 7 ( $P = 1 \text{ bar}$ ) and Fig. 8 ( $P = 5 \text{ bar}$ ). According to Landau's prediction, the data are expected to fall on a straight line with a slope of  $(\hbar/k_B)^2 = 5.83 \times 10^{-5} \text{ (mK/MHz)}^2$ . With a nonlinear least-squares fit of the 1 bar results, where each data point is weighted by the inverse square of its uncertainty, the slope of the fitting line is  $(1.3 \pm 0.3)(\hbar/k_B)^2$ , and this result is consistent with Landau's prediction. The error limits that are given encompass all of the theoretical and

experimental uncertainties including the non-parallelism, the pressure, the value of  $\alpha'(P)$ , and the path length,  $\ell$ . An unconstrained fit of the 5 bar data gives an unphysical negative slope, which means that we have not taking into account a source of attenuation in the first sound regime at this pressure. Constraining the fit to omit non-negative results yields a slope of  $(0.0 \pm 1.4)(\hbar/k_B)^2$  at 5 bar. The quantity that is most uncertain at 5 bar is the second term in the longitudinal viscosity,  $\Gamma_2$  (see Eq. (12)), and our assumptions about its pressure dependence may be responsible for the large uncertainty at 5 bar.

If the viscosity is taken by an interpolation of the data of Bertinat *et al.*<sup>29</sup> and Carless *et al.*<sup>43</sup> as was done by Granroth *et al.*,<sup>28</sup> rather than from Eq. (11), then the present data would yield a slope of  $(6.2 \pm 0.6)(\hbar/k_B)^2$  at 1 bar. This value is consistent with the  $(5.6 \pm 1.2)(\hbar/k_B)^2$  result reported by Granroth *et al.* However, it is important to stress that both of these values arise from analysis that employs a form of the viscosity that provides a poor description of the attenuation of first sound, as discussed at the end of Section VI. Consequently, the present work is an improvement over the older results due to number of reasons, including a more thorough study of the attenuation of first sound.

## IX. CONCLUSIONS

In conclusion, to within one deviation of the overall uncertainty of the measurements, the results at 1 bar agree with the predicted quantum term in zero sound predicted by Landau. The corresponding data and analysis at 5 bar yield relatively large uncertainties and consequently provide a null result for the measurement of the quantum term. The overall uncertainty at 5 bar arises mainly from the lack of a detailed knowledge of the second term in the longitudinal viscosity. Nevertheless, it is noteworthy that a similar result was obtained by Matsumoto *et al.*,<sup>26</sup> who measured the predicted quantum term at 1 bar and a null result at 5 bar. Improvements in measuring the absolute attenuation over expanded frequency and pressure ranges are required to make further progress on this fundamental issue.

## APPENDIX A: QUASIPARTICLE SCATTERING AMPLITUDE

In the zero sound regime and after subtracting the electrical crosstalk, the received signal was integrated inside the 4  $\mu$ s window corresponding to the received pulse, Fig. 2. Neglecting

the possible attenuation coming from the quantum limit, the integrated amplitude,  $\mathcal{A}$ , may be written as

$$\mathcal{A} = \beta \exp(-\alpha'(P) T^2 \ell) \quad , \quad (\text{A1})$$

where  $\alpha'(P)$  represents the contribution from quasiparticle scattering, Eq. (1). In Fig. 9, the natural logarithm of the integrated amplitude at 1 bar is plotted as a function of  $T^2$ , and the value of  $\alpha'(P)\ell$  is determined by a linear fit of this data. Since the value of  $\ell$  is established *in situ* by time-of-flight analysis (Eq. (5)), a value for  $\alpha'(P)$  may be obtained. For most frequencies, the measured values of  $\alpha'(P)$  are equal to within the experimental uncertainty, however there are slight variations due to subtle pressure changes. Similar data were obtained at 5 bar (Fig. 10), and all of the data are tabulated in Table II.

The value of  $\alpha'(P)$  can be compared to values obtained from previous experiments,<sup>16,17,18,19,20,21</sup> and Fig. 11 shows the reported values of  $\alpha'(P)$ . An alternative and perhaps physically more meaningful presentation of  $\alpha'$  is as a function of molar volume,  $\nu$ . Using the tabulated  $P(\nu)$  function,<sup>12</sup>  $\alpha'(P)$  can be converted to  $\alpha'(\nu)$ , and the results are shown in Fig. 12, where the solid line represents the results of second order polynomial fit of the data, *i.e.*

$$\alpha'(\nu) = 1.4088 - 0.14882 \nu + 4.1303 \times 10^{-3} \nu^2 \quad . \quad (\text{A2})$$

This equation can be converted back to a pressure dependence using the known  $\nu(P)$  relationship,<sup>12</sup> yielding the solid line shown in Fig. 11, *i.e.*

$$\alpha'(P) = 1.4997 - 0.15200 P + 0.010058 P^2 - 3.397 \times 10^4 P^3 + 4.3695 \times 10^6 P^4 \quad . \quad (\text{A3})$$

As far as we know, this appendix presents the first comprehensive analysis of known values of  $\alpha'$ .

## APPENDIX B: PATH LENGTH AND FIRST SOUND VELOCITY

Knowing the path length and the time delay before each received pulse, we can calculate the velocity as a function of temperature as shown in Fig. 13 for the pressure of 1 bar and 5 bar. The time delay was determined by the sudden increase of the sound amplitude corresponding to the arrival of the pulse in the 23 MHz data. The 23 MHz data was chosen because the start of the pulse is easy to identify. Received pulses with frequencies above

approximately 60 MHz appear rounded because the higher frequency harmonics of the pulse are attenuated. Within the uncertainty, the velocity is constant at both pressures. The error bars have been determined by a combination of the uncertainty in the path length and the uncertainty in the time of arrival, which is essentially one-half the time resolution of the spectrometer. In this experiment, a room temperature valve was used to access the sample space and consequently, the pressure was slightly temperature dependent due to the small volume of the  $^3\text{He}$  capillary. At 1 bar and 5 bar, the pressure changes from 100 to 800 mK are approximately 0.1 bar and 0.2 bar, respectively. This pressure change was not measured directly during this experiment, but it was observed in subsequent runs that incorporated a low temperature pressure gauge. However, because the volume of the  $^3\text{He}$  capillary is small compared to the volume of the cell, we can assume that the cell volume will remain constant. Setting of the  $^3\text{He}$  pressure was performed at the temperature of 250 mK. The molar volumes corresponding to 1 bar and 5 bar at 250 mK, determined using the results of Kollar and Vollhardt,<sup>31</sup> are 35.6516 and 32.5883 cm<sup>3</sup>, respectively. Using these constant molar volumes, the temperature dependence of all other thermodynamic quantities can then be calculated.<sup>31</sup> In Fig. 13, the triangles are calculated from the first sound velocity expression given by Roach *et al.*<sup>46</sup> using the adiabatic compressibility and density values from Kollar and Vollhardt.<sup>31</sup> These theoretical curves have been adjusted by a constant ( $-7.05$  m/s for 1 bar and  $-0.35$  m/s for 5 bar) to match the experimental velocity value at 50 mK. The solid lines represent the theoretical first sound velocity calculated using the expression given by Abraham *et al.*<sup>47</sup> Likewise, these theoretical curves have been adjusted by a constant ( $1.85$  m/s for 1 bar and  $-0.32$  m/s for 5 bar) to match the experimental velocity value at 50 mK. The first sound velocity at 250 mK given by Halperin and Varoquaux<sup>12</sup> is also shown (squares). Our fits involving the first sound velocity used the constants 200.61 m/s for 1 bar and 249.62 m/s for 5 bar.

## ACKNOWLEDGMENTS

During the course of this work, we have benefited from conversation or correspondence with D. Einzel, A. Feher, G.E. Granroth, W.P. Halperin, G.G. Ihas, Y. Lee, Y. Okuda, J. Parpia, J.A. Sauls, and the late J.R. Hook. We gratefully acknowledge N. Bushong for



assistance in preparing Fig. 1.

---

\* Present address: Information Systems Laboratories, Inc., San Diego, CA 92121, USA.

<sup>1</sup> L. D. Landau, *Sov. Phys. JETP* **3**, 920 (1957).

<sup>2</sup> L. D. Landau, *Sov. Phys. JETP* **5**, 101 (1957).

<sup>3</sup> P. Nozières, *Theory of Interacting Fermi Systems* (Benjamin, New York, 1964).

<sup>4</sup> D. Pines and P. Nozières, *The Theory of Quantum Liquids, Volume I: Normal Fermi Liquids* (Benjamin, New York, 1966); reissued (Addison-Wesley, New York, 1989).

<sup>5</sup> A. J. Leggett, *Rev. Mod. Phys.* **47**, 331 (1975).

<sup>6</sup> G. Baym and C. Pethick, in *The Physics of Liquid and Solid Helium, Part II*, K. H. Bennemann and J. B. Ketterson, eds. (Wiley and Sons, New York, 1978), p. 1. Reprinted by G. Baym and C. Pethick, *Landau Fermi-Liquid Theory* (Wiley and Sons, New York, 1991).

<sup>7</sup> D. Vollhardt and P. Wölfle, *The Superfluid Phases of Helium 3* (Taylor & Francis, London, 1990).

<sup>8</sup> E. R. Dobbs, *Helium Three* (Oxford University Press, Oxford, 2000).

<sup>9</sup> One of the important predictions of the theory was the linear temperature dependence of the normal liquid heat capacity at temperatures small compared to the Fermi temperature,  $T_F$ . This prediction was first experimentally observed in 1966 by Abel, Anderson, Black, and Wheatley.<sup>10</sup> Later in other work, Greywall utilized this theoretical prediction in the form of a physical “law” to calibrate an LCMN thermometer bathed in normal liquid  $^3\text{He}$  at low pressure.<sup>11</sup> Greywall used this thermometer to establish a normal liquid-superfluid phase diagram,  $T_c(P)$ ,<sup>11</sup> which has been used extensively.<sup>12</sup> However, it is noteworthy, albeit not explicitly a concern of this paper, that ultrasonic studies of superfluid  $^3\text{He}$  suggest that  $T_c(P)$  is not well determined at pressures below 10 bar.<sup>13,14</sup>

<sup>10</sup> W. R. Abel, A. C. Anderson, W. C. Black, and J. C. Wheatley, *Phys. Rev.* **147**, 111 (1966).

<sup>11</sup> D. S. Greywall, *Phys. Rev. B* **33**, 7520 (1986).

<sup>12</sup> W. P. Halperin and E. Varoquaux, *Helium Three*, edited by W. P. Halperin and L. P. Pitaevskii (North-Holland, Amsterdam, 1999) p. 510.

<sup>13</sup> R. Movshovich, N. Kim, and D. M. Lee, *Phys. Rev. Lett.* **64**, 431 (1990).

<sup>14</sup> N. Masuhara, B. C. Watson, and M. W. Meisel, *Phys. Rev. Lett.* **85**, 2537 (2000).

- <sup>15</sup> B. E. Keen, P. W. Matthews, and J. Wilks, *Phys. Lett.* **5**, 5 (1963); *Proc. Roy. Soc. (London)* **A284**, 125 (1965).
- <sup>16</sup> W. R. Abel, A. C. Anderson, and J. C. Wheatley, *Phys. Rev. Lett.* **17**, 74 (1966).
- <sup>17</sup> D. T. Lawson, W. J. Gully, S. Goldstein, R. C. Richardson, and D. M. Lee, *Phys. Rev. Lett.* **30**, 541 (1973); *J. Low Temp. Phys.* **15**, 169 (1974).
- <sup>18</sup> J. B. Ketterson, P. R. Roach, B. M. Abraham, and P. D. Roach, *Quantum Statistics and the Many Body Problem*, edited by S. B. Trickey, W. P. Kirk, and J. W. Dufty (Plenum, New York, 1975) p. 35.
- <sup>19</sup> D. B. Mast, B. K. Sarma, J. R. Owers-Bradley, I. D. Calder, J. B. Ketterson, and W. P. Halperin, *Phys. Rev. Lett.* **45**, 266 (1980).
- <sup>20</sup> K. Nara, I. Fujii, K. Kaneko, and A. Ikushima, *Physica B* **108**, 1203 (1981).
- <sup>21</sup> O. Avenel and E. Varoquaux, private communication (1984).
- <sup>22</sup> A. A. Abrikosov and I. M. Khalatnikov, *Rep. Prog. Phys.* **22**, 329 (1959).
- <sup>23</sup> J. Wilks, *The Properties of Liquid and Solid Helium* (Clarendon Press, Oxford, 1967), Sec. 18.4.
- <sup>24</sup> J. W. Serene and D. Rainer, *Phys. Rep.* **101**, 221 (1983).
- <sup>25</sup> K. Matsumoto, T. Ikegami, and Y. Okuda, *Physica B* **195-196**, 743 (1994).
- <sup>26</sup> K. Matsumoto, T. Ikegami, K. Karaki, and Y. Okuda, *Czech. J. Phys.* **46**, Suppl. S1, 63 (1996).
- <sup>27</sup> C. Barre, J. Y. Prieur, J. Joffrin, M. Stenger, and M. Chapellier, *Physica B* **219-220**, 663 (1996).
- <sup>28</sup> G. E. Granroth, N. Masuhara, G. G. Ihas, and M. W. Meisel, *J. Low Temp. Phys.* **113**, 543 (1998).
- <sup>29</sup> M. P. Bertinat, D. S. Betts, D. F. Brewer, and G. J. Butterworth, *J. Low Temp. Phys.* **16**, 479 (1974).
- <sup>30</sup> M. Nakagawa, A. Matsubara, O. Ishikawa, T. Hata, and T. Kodama, *Phys. Rev. B* **54**, R6849 (1996).
- <sup>31</sup> M. Kollar and D. Vollhardt, *Phys. Rev. B* **61**, 15347 (2000).
- <sup>32</sup> J. Sykes and G. A. Brooker, *Ann. of Phys. NY* **56**, 1 (1970).
- <sup>33</sup> N. Masuhara, B. C. Watson, and M. W. Meisel, *J. Low Temp. Phys.* **121**, 815 (2000).
- <sup>34</sup> B. C. Watson, Ph. D. thesis, University of Florida (2000), unpublished.
- <sup>35</sup> J. Xu, O. Avenel, J. S. Xia, M. F. Xu, T. Lang, P. L. Moyland, W. Ni, E. D. Adams, G. G. Ihas, M. W. Meisel, N. S. Sullivan, and Y. Takano, *J. Low Temp. Phys.* **89**, 719 (1992).

- <sup>36</sup> M. W. Meisel, G. R. Stewart, E. D. Adams, *Cryogenics* **29**, 1168 (1989).
- <sup>37</sup> W. Ni, J. S. Xia, E. D. Adams, P. S. Haskins, and J. E. McKisson, *J. Low Temp. Phys.* **99**, 167 (1995); W. Ni, Ph. D. thesis, University of Florida (1994), unpublished.
- <sup>38</sup> E. R. Grilly, *J. Low Temp. Phys.* **4**, 615 (1971).
- <sup>39</sup> L. D. Landau and E. M. Lifshitz, *Fluid Mechanics* (Pergamon Press, Oxford, 1959).
- <sup>40</sup> D.S. Greywall, *Phys. Rev. B* **29**, 4933 (1984).
- <sup>41</sup> G. Eska, K. Neumaier, W. Schoepe, K. Uhlig, and W. Wiedemann, *Phys. Rev. B* **27**, 5534 (1983).
- <sup>42</sup> M. A. Black, H. E. Hall, and K. Thompson, *J. Phys. C: Solid State Phys.* **4**, 129 (1971).
- <sup>43</sup> D. C. Carless, H. E. Hall, and J. R. Hook, *J. Low Temp. Phys.* **50**, 583 (1983).
- <sup>44</sup> B. M. Abraham, Y. Eckstein, J. B. Ketterson, M. Kuchmir, and P. R. Roach, *Phys. Rev.* **181**, 347 (1969); B. M. Abraham, Y. Eckstein, J. B. Ketterson, M. Kuchmir, and P. J. Vignos, *Phys. Rev. A* **1**, 250 (1970).
- <sup>45</sup> R. Truell, C. Elbaum, and B. B. Chick, *Ultrasonic Methods in Solid State Physics* (Academic Press, New York, 1969).
- <sup>46</sup> P. R. Roach, Y. Eckstein, M. W. Meisel, and L. Aniola-Jedrzejek, *J. Low Temp. Phys.* **52**, 433 (1983).
- <sup>47</sup> B. M. Abraham, D. Chung, Y. Eckstein, J. B. Ketterson, and P. R. Roach, *J. Low Temp. Phys.* **6**, 521 (1972).

Reference	$\omega/2\pi$ (MHz)	$T_{min}$ (mK)	$P$ (bar)	$\left(\frac{\hbar\omega}{2\pi k_B T_{min}}\right)^2$
Matsumoto <i>et al.</i> <sup>25</sup>	389	2.5	3	0.11
Matsumoto <i>et al.</i> <sup>26</sup>	389	6	0.4	0.25
	389	6	3	0.25
	389	7	5	0.18
Barre <i>et al.</i> <sup>27</sup>	84	7	SVP	0.01
	254	7	SVP	0.08
	422	7	SVP	0.21
	592	7	SVP	0.42
Granroth <i>et al.</i> <sup>28</sup>	46	1.08	1	0.11
This Work	23	1.11	1	0.03
	67	1.11	1	0.21
	107	1.11	1	0.54
	28	1.55	5	0.02
	68	1.55	5	0.11
	108	1.55	5	0.28

TABLE I: Summary of studies made at high frequency and low temperature. Listed for each experiment are the frequency, the minimum temperature, the pressure, and the relative value of the predicted quantum term in the zero sound attenuation (Eq. (3)). The notation “SVP” means “saturated vapor pressure”.

$(\omega/2\pi)$ (MHz)	$\alpha'(P = 1 \text{ bar})$ ( $\text{cm}^{-1}$ )	$\alpha'(P = 5 \text{ bar})$ ( $\text{cm}^{-1}$ )
8		$0.91 \pm 0.05$
10	$1.25 \pm 0.04$	$0.80 \pm 0.04$
16	$1.31 \pm 0.02$	$0.86 \pm 0.04$
19	$1.30 \pm 0.04$	
20	$1.33 \pm 0.03$	$0.93 \pm 0.05$
21	$1.30 \pm 0.04$	
22	$1.34 \pm 0.02$	
23	$1.32 \pm 0.01$	$0.83 \pm 0.04$
28		$0.76 \pm 0.04$
63	$1.34 \pm 0.03$	$0.94 \pm 0.05$
64	$1.34 \pm 0.01$	$0.84 \pm 0.03$
65	$1.31 \pm 0.04$	$0.94 \pm 0.05$
66	$1.28 \pm 0.02$	
66.6	$1.35 \pm 0.02$	$0.86 \pm 0.02$
68		$0.89 \pm 0.07$
107	$1.4 \pm 0.1$	$0.9 \pm 0.1$
108	$1.25 \pm 0.05$	$0.99 \pm 0.02$
Average	$1.32 \pm 0.01$	$0.88 \pm 0.02$

TABLE II: The values of  $\alpha'(P)$ , Eqs. (1) and (16), as determined from a linear fit to the data when plotted in the manner shown in Figs. 9 and 10.

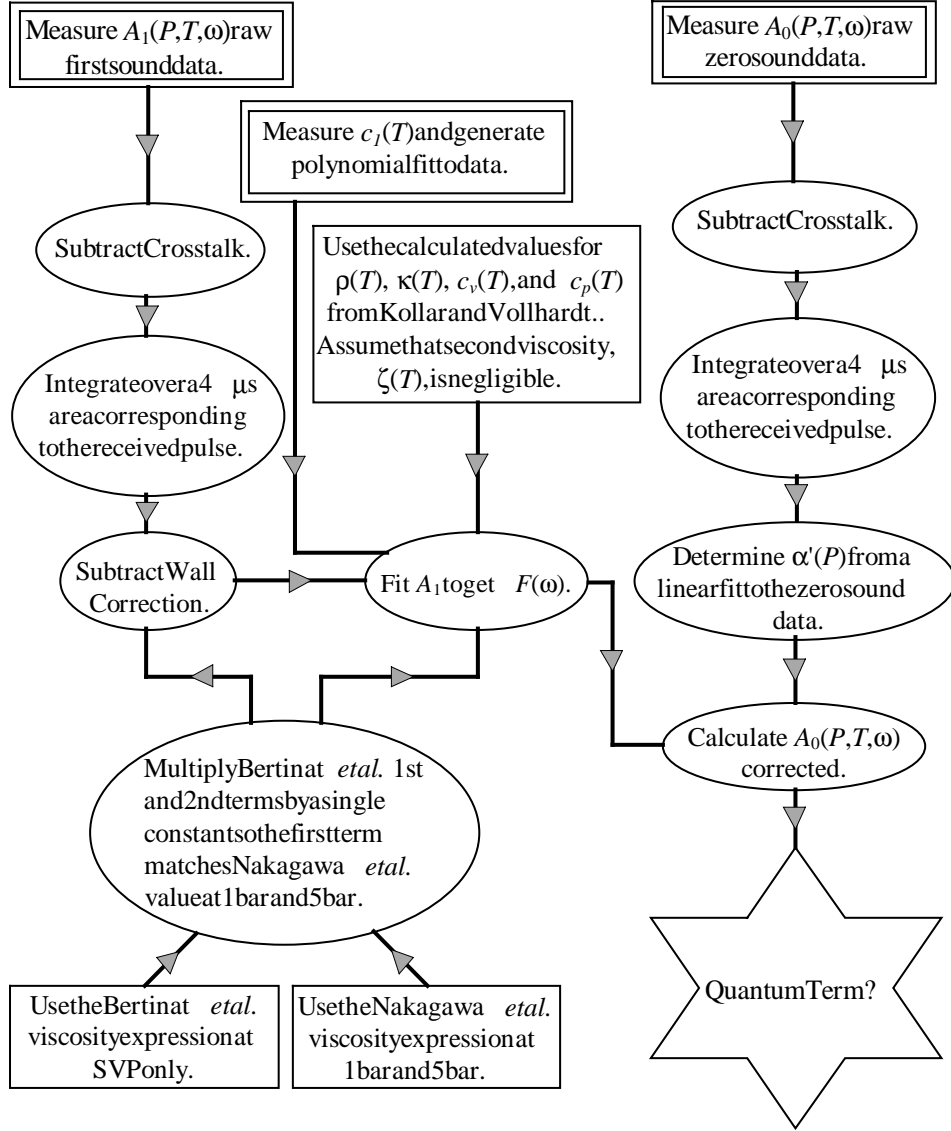


FIG. 1: Flow diagram depicting the process used to analyze the data. Input data from our measurements are represented by double rectangles, and mathematical operations are shown by ellipses. Input about the properties of the liquid are bounded by rectangles, and this information was taken from Bertinat *et al.*,<sup>29</sup> Nakagawa *et al.*,<sup>30</sup> and Kollar and Vollhardt.<sup>31</sup>

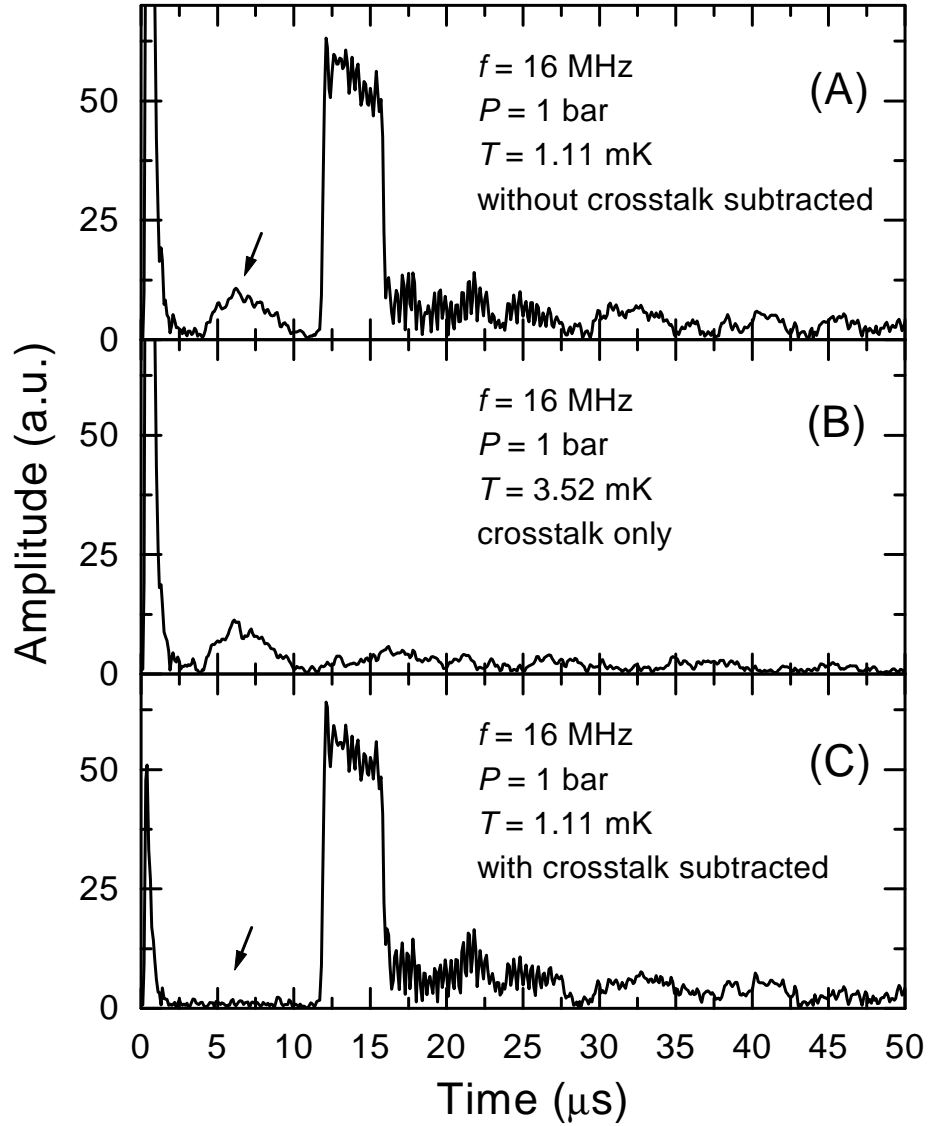


FIG. 2: The received amplitude of a 16 MHz pulse as a function of time at a pressure of 1 bar and a temperature of 1.11 mK. In (A), the coherent noise due to electrical feedthrough is evident in the first 10  $\mu\text{s}$  of data. At a temperature of 3.52 mK (B), the signal is attenuated and only the crosstalk remains. In (C), the result of subtracting (B) from (A) is shown.

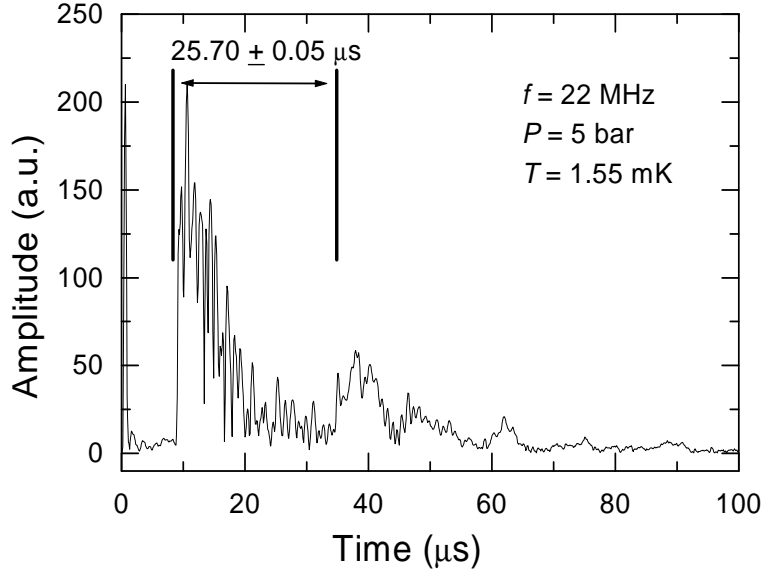


FIG. 3: A 22 MHz received pulse, at 5 bar and 1.55 mK, as a function of time. The time length between the first received pulse and the first echo is shown.

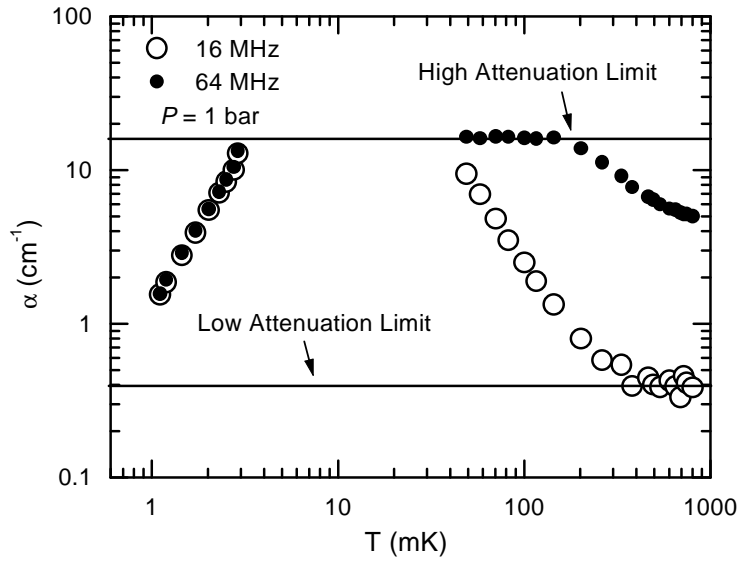


FIG. 4: The dynamic range of our measurement of the sound attenuation as a function of the temperature at 1 bar. The upper horizontal line indicates the high attenuation limit where the signal is too small to be detected. The lower horizontal line indicates the signal level where changes in the attenuation are smaller than the noise.



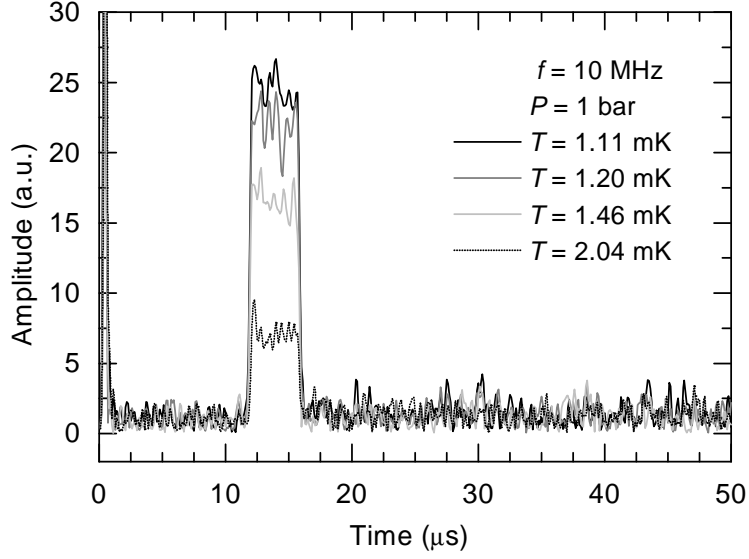


FIG. 5: Typical received pulse amplitudes as a function of time and temperature for a zero sound pulse at 10 MHz and 1 bar. The crosstalk has been subtracted.

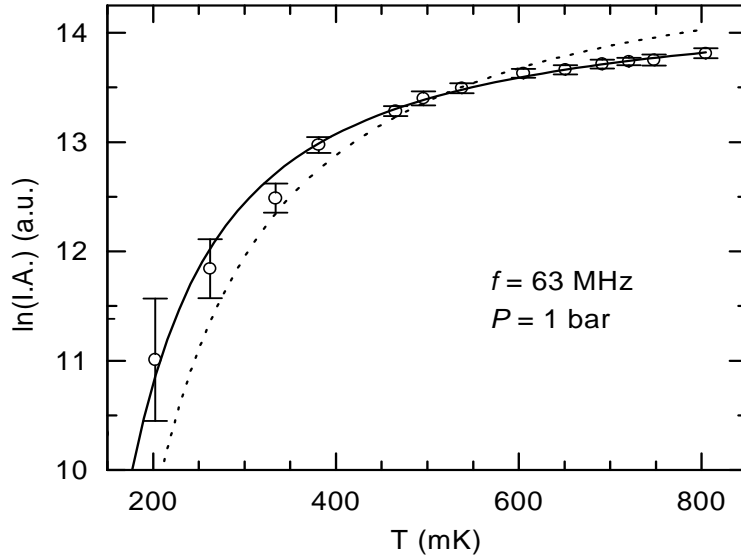


FIG. 6: The natural logarithm of the integrated amplitude,  $\ln(I.A.)$  in arbitrary units, is plotted as a function of temperature at 63 MHz and 1 bar. The solid line is generated when using the viscosity given by Eq. (11). The dotted line arises when using viscosity values interpolated from other work,<sup>29,43</sup> and this approach was used by Granroth *et al.*<sup>28</sup>

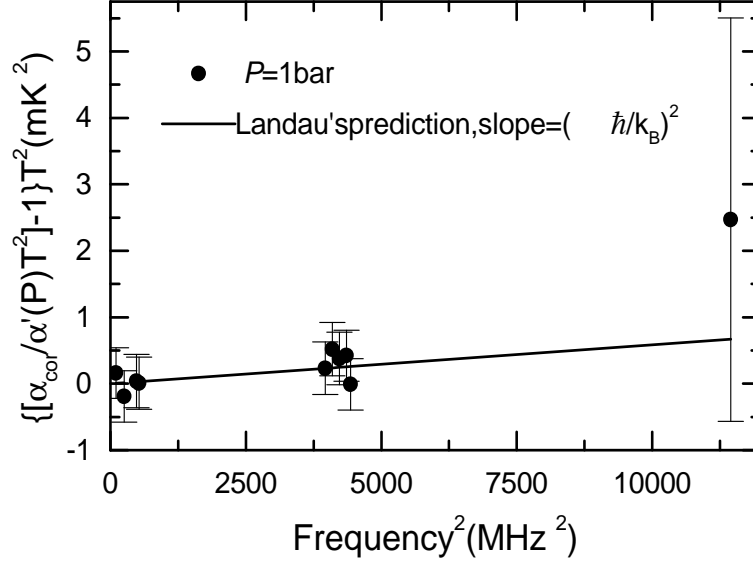


FIG. 7: The corrected and normalized attenuation at 1 bar plotted as a function of the square of the frequency, Eq. (1). The data yield a slope of  $(1.3 \pm 0.3)(\hbar/k_B)^2$ .

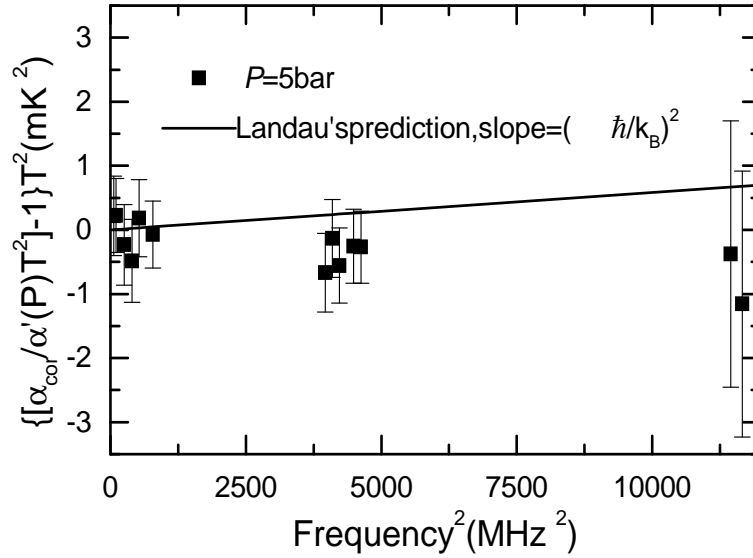


FIG. 8: The corrected and normalized attenuation at 5 bar plotted as a function of the square of the frequency, Eq. (1). The data yield a slope of  $(0.0 \pm 1.4)(\hbar/k_B)^2$ .

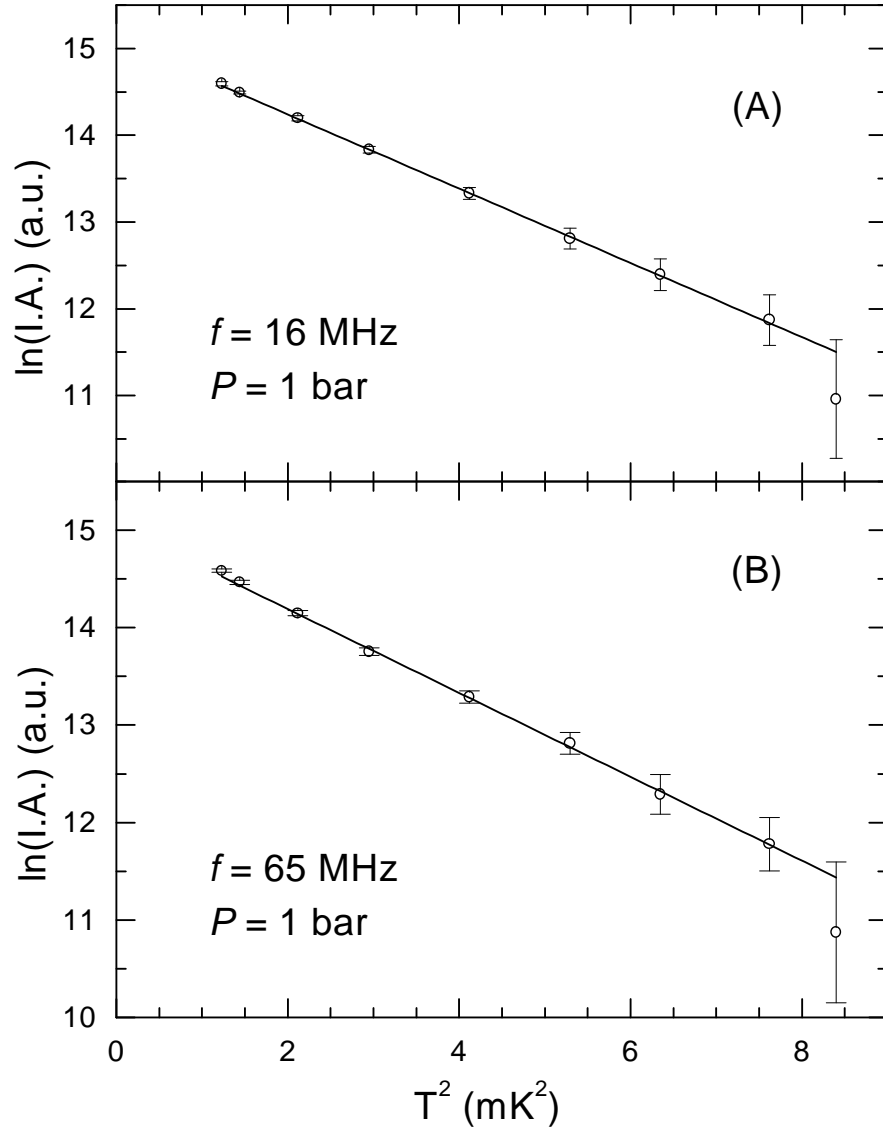


FIG. 9: Typical data for the natural logarithm of the integrated amplitude (I.A.) in arbitrary units as a function of  $T^2$  at 1 bar.

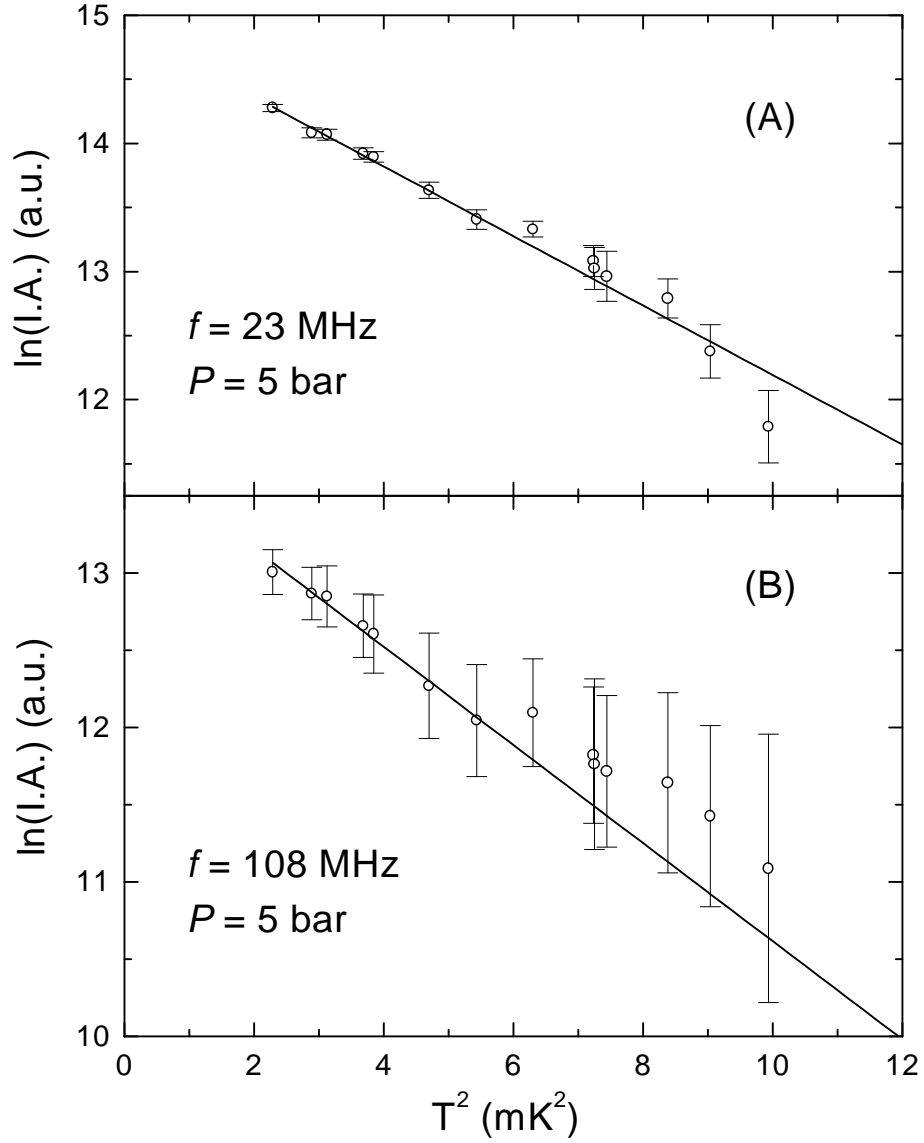


FIG. 10: Typical data for the natural logarithm of the integrated amplitude (I.A.) in arbitrary units as a function of  $T^2$  at 5 bar.

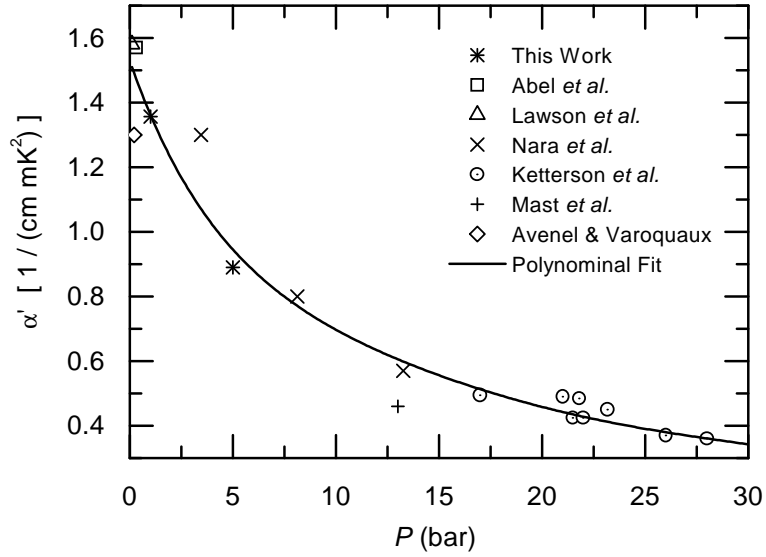


FIG. 11: The values of  $\alpha'$ , Eq. (1), as measured by our work and other researchers.<sup>16,17,18,19,20,21</sup> The solid line is from Eq. (A3), see text.

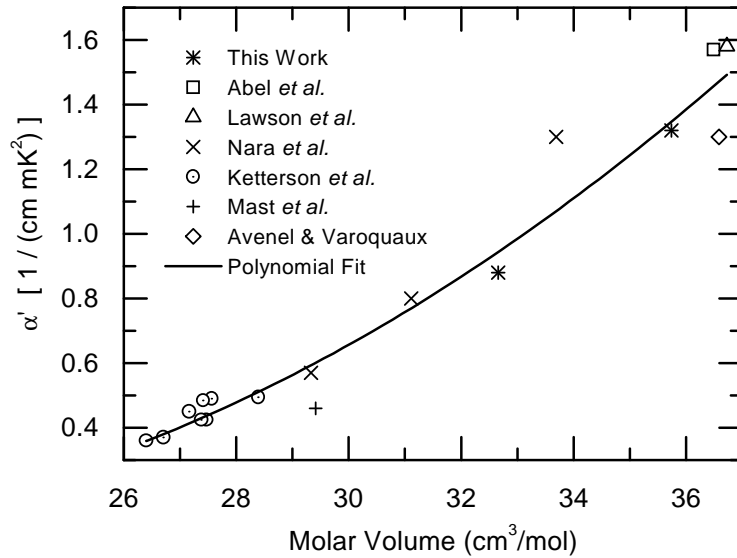


FIG. 12: The values of  $\alpha'(P)$  shown in Fig. 11 have been converted to a function of molar volume using known values of  $P(\nu)$ .<sup>12</sup> The solid line is from Eq. (A2) which is a fit of the data.

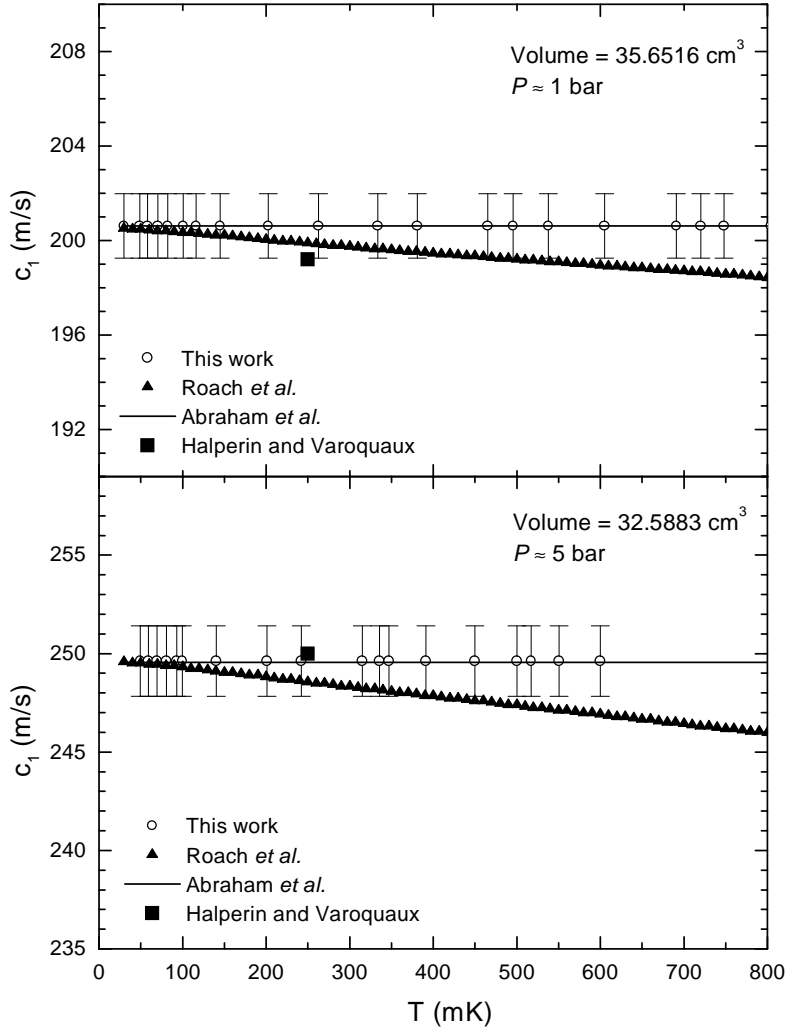


FIG. 13: The velocity of first sound as a function of temperature at a pressure of 1 bar and 5 bar calculated using the path length and the measured signal delay for a 23 MHz pulse. The results of Roach *et al.*<sup>46</sup> and Abraham *et al.*<sup>47</sup> require input that was obtained from Kollar and Vollhardt,<sup>31</sup> and also involve smaller shifts to normalize all the data to the values at 50 mK, see text. The values as tabulated by Halperin and Varoquaux<sup>12</sup> do not involve any additional input parameters or shifts.